Progress In Electromagnetics Research M, Vol. 107, 181–191, 2022

Compact, Dual-Polarized, Oblong Loop Antenna for 5G Laptops

Saou-Wen Su*

Abstract—A compact, two-port, oblong loop antenna producing two orthogonal waves for fifth-generation (5G) operation in the 3.4–3.6 GHz band with transmission coefficient (S_{12}) lower than −32 dB and excellent envelope correlation coefficient (ECC) less than 0.002 is introduced for laptop antenna applications. Unlike the conventional, probe-fed, dual-polarized patch antennas, the proposed design uses the loop antenna fed by the coaxial cables and has a coplanar structure. The loop antenna is placed 1 mm above the top edge of the display, has a compact size of 30 mm × 4 mm and two feed ports spaced merely 2 mm (about 0.02-λ at 3.4 GHz) apart. Port1 is designed as a coupling feed to the loop while port2 is a direct feed in the loop, all located along the loop's central line. With this feeding arrangement, port2 is located in the current-null region when port1 is excited, whereas maximum currents of port1 excitation are located in the current nulls of port2 excitation. These properties lead to two decoupled, orthogonal radiating waves with very low ECC. Additionally, due to the oblong structure of the loop, pattern diversity is also achieved. Details of the dual-polarized loop antenna for 5G applications are presented.

1. INTRODUCTION

Dual-polarized microstrip/patch antennas have been excessively studied and designed to increase the capacity in wireless communications. These designs usually utilize a single square or oblong radiating patch excited by two orthogonal feed ports with a particular feeding method to produce two orthogonal, decoupled radiating waves [1–5]. In these design cases, the patch's two broadside radiation patterns in the E- and H-planes with polarization diversity are obtained. Also, it is noteworthy that by exciting different resonant modes of the same patch, broadside and conical radiation patterns with pattern diversity can be achieved for dual-polarized patch antennas [6–9]. However, to function at the same frequencies, the modified patch structures or use of the external feeding networks become necessary, which make these designs more complicated.

In this paper, the antenna type is substantially different from the conventional, dual-polarized patch antennas using two orthogonal feed ports for polarization diversity [1–5] or exciting different resonant modes for pattern diversity [6–9]. Instead, a simple, dual-polarized oblong loop antenna is proposed for producing two uncorrelated waves for orthogonal polarization and pattern diversity in the laptop computer. To the author's best knowledge, no or very scant studies using loops to achieve dual-polarization and pattern-diversity properties are available in the literature. Compared with the patch designs [1–9], the proposed loop design has a coplanar structure and can be easily fed using the coaxial cable (unlike bulky probe feed for patch). These attractive features are favorable for practical laptop antennas. A comparison table of the cited work [1–9] is provided in Table 1.

The proposed oblong loop is printed on a single-layered substrate placed above the laptop display and fed by one coupling feed (port1) and one direct feed (port2) along the loop's geometry central

Received 25 November 2021, Accepted 17 January 2022, Scheduled 21 January 2022

* Corresponding author: Saou-Wen Su (Saou-Wen_Su@asus.com).
The author is with the Antenna Design Department, Advanced EM & Wireless Communication R&D Center ASUS, Taipei 11259, Taiwan.

Table 1. Comparison of the cited work [1–9]. λ_0 is the free-space wavelength at the designed center frequency. Isolation is the negative value of transmission coefficient [29].

Ref.	Center frequency	Antenna size	Diversity/Radiating waves	Isolation dB
1	10 GHz	0.28-λ × 0.28-λ	dual-polarization/broadside	> 24
2	1.8 GHz	0.35-λ × 0.35-λ	dual-polarization/broadside	> 35
3	1.8 GHz	0.37-λ × 0.37-λ	dual-polarization/broadside	> 30
4	3.4 GHz	0.34-λ × 0.34-λ	dual-polarization/broadside	> 34
5	4 GHz	0.40-λ × 0.40-λ	dual-polarization/broadside	> 38
6	2.1 GHz	0.40-λ (*circular**)	pattern/broadside and conical	> 24
7	2.44 GHz	0.44-λ (*circular**)	pattern/broadside and conical	> 40
8	2.1 GHz	0.39-λ (*circular**)	pattern/broadside and conical	> 15
9	3.5 GHz	0.59-λ (*circular**)	pattern/broadside and conical	> 13
Proposed	3.5 GHz	0.02-λ × 0.47-λ	dual-polarization and pattern /broadside and dipole-like	> 32

*Size represents the diameter of the circular microstrip/patch antennas

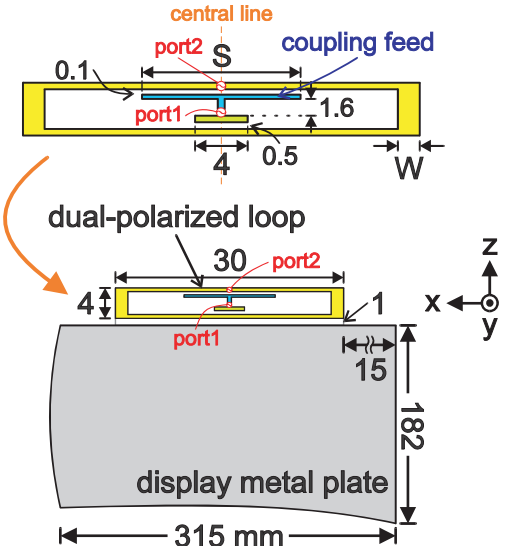

Figure 1. Geometry of the dual-polarized loop antenna for laptop antenna applications.

line (see Fig. 1). In addition, because the current null excited by port1 occurs at the position of port2, whereas the maximum currents by port1 are located in the current nulls of port2 excitation, low transmission coefficient lower than −32 dB can be achieved for low mutual coupling between two antenna ports.

To demonstrate the dual-polarized loop-design concept, the prototyped example functioning for fifth-generation (5G) operation in the 3.4–3.6 GHz band [10] is studied and validated. The design is of a simple oblong loop, which has a lateral length of 30 mm and a small profile of 4 mm (about 0.04-λ at 3.4 GHz), making it suitable for the laptop computer with a narrow display bezel (mostly 5 to 6 mm) [11–15]. In this loop design, the two one-wavelength loop modes can be excited simultaneously

and show 90 degree phase difference, which leads to two decoupled, orthogonal radiating waves with very low correlation less than 0.002 in the far-field radiation patterns. In addition, the patterns of the two-port excitation resemble those of one dipole along the $\pm z$ axes and one dipole along the $\pm x$ axes above a relatively large ground plane.

This paper is organized as follows: Section 2 first describes the design structure of the dual-polarized loop antenna. A proof-of-concept prototyped example is discussed in simulation and experimentally verified for its impedance and radiation characteristics in Section 3. Finally, the conclusion is given in Section 4. Details of the antenna design are described and discussed.

2. TWO-PORT, DUAL-POLARIZED LOOP DESIGN

Figure 1 shows the proposed, two-port, dual-polarized loop design for laptop antenna applications. A fabricated prototype photo is shown in Fig. 2. The oblong loop design of size 30 mm × 4 mm (about $0.34\lambda \times 0.04\lambda$ at 3.4 GHz) is placed 1 mm above the metal plate of size 315 mm × 182 mm × 1 mm, regarded as a 14-inch laptop display ground plane. The antenna dimensions were parametrically optimized to function in the 3.4–3.6 GHz 5G band with the aid of the full-wave simulator, Ansys HFSS [16]. Two antenna ports are aligned with the geometry central line with a port-to-port distance of merely 2 mm (about 0.02-λ at 3.4 GHz) to excite the loop's two one-wavelength resonant modes. Note that the overall design height of 5 mm, including the gap between the loop and the display ground, makes it possible for the proposed design to be embedded within the narrow bezel (mostly 5 to 6 mm) of laptop computers. Two 50-Ω mini-coaxial cables with each attached around by a balun (not shown in the photo of Fig. 2) were used for feeding the loop. Note that to alleviate the cable effects, the avoidance of overlapping the two coaxial cables over the antenna, as seen in Fig. 2, is critical to the measured results.

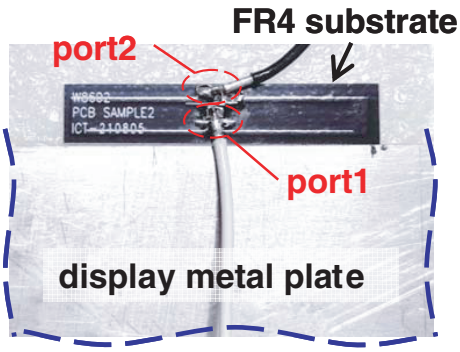

Figure 2. Photo of a fabricated prototype.

The fabricated prototype is printed on a flame retardant 4 (FR4) substrate, which has a thickness 0.4 mm, relative permittivity 4.4, and loss tangent 0.024. A coupling feed for the loop's port1 is first designed by using a T strip (width of 0.3 mm) and has a tiny coupling gap of 0.1 mm to the loop's longer edge. Opposite the middle of the T strip, the loop is directly fed by port2. For simplicity, the loop strip is set with a constant width of 0.5 mm and has two widened portions (width W) at the two shorter edges. The horizontal length S of the coupling strip has more effects on tuning the resonant frequencies for port1 excitation while the loop width W at the two shorter edges can affect both port1 and port2 operating frequencies.

The design methodology is summarized as follows. The first step is to feed a one-wavelength close-form loop by using a coupling feed (port1). This gives rise to a current null right opposite the feeding strip. Then, for minimum impacts on port1, a direct feed (port2) is inserted in the position of the current null of port1 excitation. In this case, dual-polarization and pattern diversity are attained. Finally, the parameters of the feeding strip and the widened portions at the loop's shorter edges are fine tuned to obtain the same in-band frequencies for the two feed ports. The operating principle for the dual-polarized loop will be elaborated in detail in the following section.

3. RESULTS AND DISCUSSIONS

3.1. Reflection Coefficients, Transmission Coefficient, and TARC

Figure 3 shows the measured and simulated reflection coefficients (S_{11} for port1, S_{22} for port2) and the transmission coefficient (S_{12} between port1 and port2) for the prototype based upon the dimensions described in Fig. 1. All simulation studies in this paper are conducted using Ansys HFSS. The simulated data on average agree well with the experimental results. With the impedance matching better than -6 dB (VSWR of 3), the reflection coefficients cover the 3.4–3.6 GHz band. Note that the -6 dB impedance is usually defined for 5G mobile antennas as shown in [17–23]. Additionally, owing to the orthogonal polarization between the loop's two ports, low transmission coefficient lower than -32 dB is also achieved.

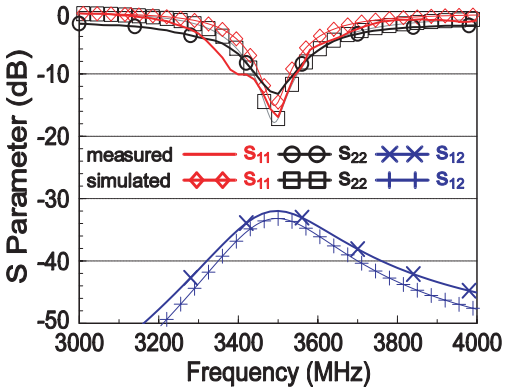

Figure 3. Measured and simulated reflection and transmission coefficients (S_{11} for port1, S_{22} for port2, S_{12} between port1 and port2) of the proposed design; $S = 12$ mm, $W = 1.65$ mm.

Figure 4 shows the simulated S-parameters of port1 and port2 in the proposed design and the cases of port1 only and port2 only. The dimensions are kept the same. The impedance matching of port1 in the proposed design is almost the same as that of port1 only. As for port2 in the proposed design, the impedance bandwidth is slightly larger than that of port2 only by 20 MHz. The unaffected impedance bandwidths of port1 only and port2 only are largely attributed to very low transmission coefficient between two ports. Nevertheless, these indicate that both good port decoupling and acceptable matching are obtained for the proposed, dual-polarized loop design.

Figures 5 and 6 give the S parameters for the proposed design as a function of the length S of the coupling feed and the width W of the tuning portion, respectively. In Fig. 5, the coupling length S has negligible effects on port2's impedance bandwidth but rather affects port1's resonant frequencies. The longer the length S is, the lower the port1 frequency becomes. For the width W of the tuning portion, it is located in strong current positions for port1 excitation whereas in current-null regions for port2, it can impact both port1 and port2 frequencies. It is noteworthy that for the loop antenna design, an increase in the strip width in the strong current portions increases the loop's operating frequencies [24] while the increased width in the current-null regions leads to decreased frequencies [25]. These phenomena can also be found for the proposed loop in Fig. 6. Overall, from the results of Figs. 5 and 6, the width W of the tuning portion needs to be fixed first for por2 excitation, and then, the frequencies of port1 can be fine-tuned by using the length S of the coupling strip.

The coupling feed gap of the T strip to the proposed loop was also analyzed. It much affects the reflection coefficient of port1 as the coupling feed is used for port1 excitation (but the antenna frequencies are not much changed for port2). When the gap increases from 0.1 to 0.3 mm, the port1 frequencies also shift toward higher frequencies from 3.49 to 3.61 GHz, and the impedance matching also becomes better (real part moves from 36 to 49 Ω). However, increased frequencies will lead to the increasing size of the antenna, which is unwanted in this design. In the interest of brevity, the related

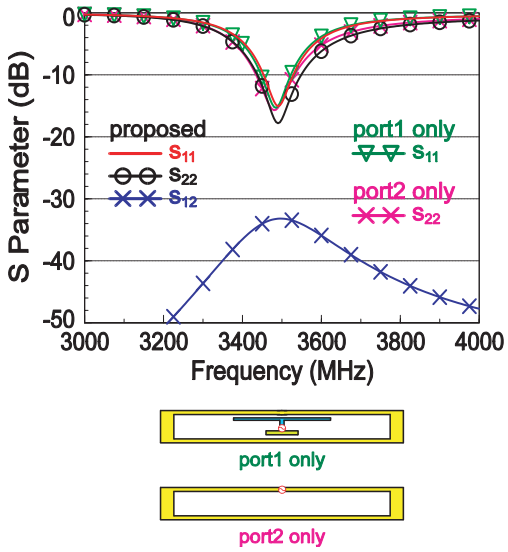

Figure 4. Simulated S parameters (S_{11} for port1, S_{22} for port2, S_{12} between port1 and port2) of the proposed design, port1 only, and port2 only.

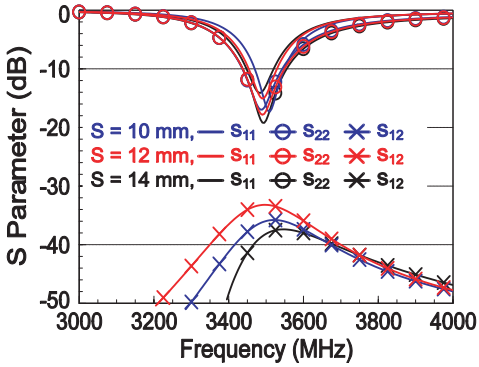

Figure 5. Simulated S parameters as a function of the coupling feed length S.

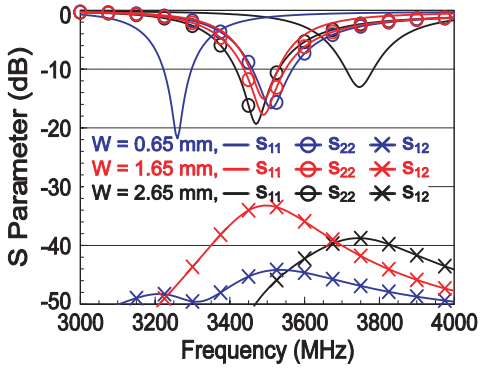

Figure 6. Simulated S parameters as a function of the tuning portion width W.

results are not presented in the article.

$$\Gamma_a^t = \sqrt{(|(S_{11} + S_{12}e^{j\theta})|^2) + |(S_{21} + S_{22}e^{j\theta})|^2} \Big/ \sqrt{2} \tag{1}$$

The total active reflection coefficients (TARC) for the proposed dual-polarized loop are also investigated. The calculations can be derived from using the scattering matrix of the lossless multiple antennas as described in [26–29], assuming Gaussian and multipath spread in multi-input multi-output (MIMO) propagation channels. This figure of merit considers random-phased signals coupled with combinations of each port's reflected signals in the antenna array. In the case of the two antennas, the TARC can be evaluated by using Eq. (1) [27–29]. Fig. 7(a) shows the TARC for port1 excitation with randomly phased port2 with a set of seven excitation vectors (phase angle from 0 to 180 degrees), and the TARC, for the other way around, for port2 excitation with randomly phased port1 is given in Fig. 7(b). Not much variation in the TARC curves is seen with the bandwidths similar to that of single port excitation in the two-port loop. For example, the TARC in Fig. 7(b) retains similar properties of port2 excitation (S_{22}) with port1 terminated to a 50 Ω load. The unaffected results are largely owing to very low transmission coefficient (S_{12}) between port1 and port2 in this design.

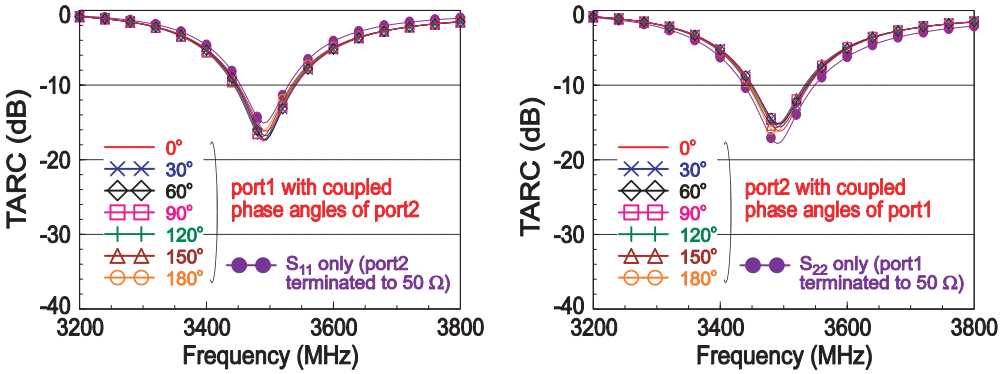

Figure 7. Calculated TARC for (a) port1 and (b) port2 with constant amplitude but different phase angles of its port counterpart (port1 and port2) in steps of 30 degrees for 180 degrees.

3.2. Surface Current Distribution, Radiation Characteristics, and ECC

Figure 8 shows the simulated current distribution for port1 and port2 excitation at 3.5 GHz for the proposed dual-polarized loop. First, two current nulls are found, when port1 is excited, on the loop's longer edges and along the central line. By contrast, for port2 excitation, the nulls occur on the shorter edges of the loop. Specifically, two one-wavelength loop modes with possible orthogonal radiating waves can be attained. Moreover, port2 is located in the position of one current null when port1 is excited while port1's strong surface currents are seen in port2's current-null regions. These properties make the proposed, two-port loop design achieve good port decoupling.

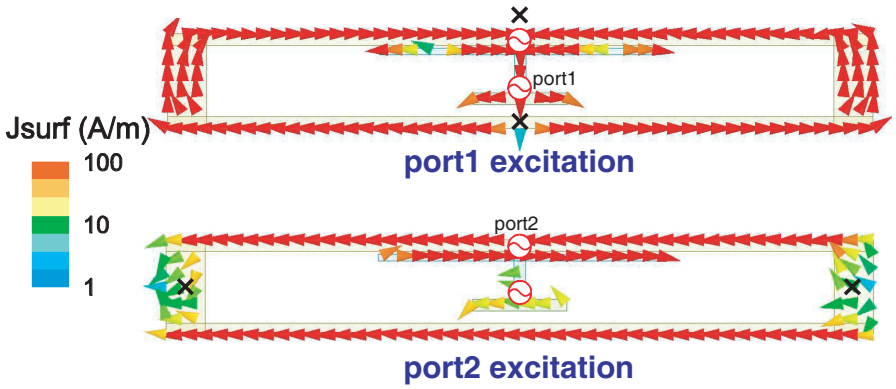

Figure 8. Simulated surface current distribution of port1 and port2 of the proposed design excited at 3.5 GHz.

Figure 9(a) shows the vector electric field distribution in the antenna plane (that's the x-z plane defined by the antenna coordinate shown in Fig. 1) for the proposed loop at 3.5 GHz. The electric fields surrounding the loop above the display ground for port1 and port2 simultaneous excitation show 90 degree phase difference coupled with two orthogonal radiating waves. The electric field of port1 is in the vertical direction with relatively large field (see dashed circle line in the figure) right above the middle of the loop's longer edges. On the other hand, the strong electric fields exist around the loop's two shorter edges with horizontal field dominant for port2 excitation. These properties not only reflect the current distribution shown in Fig. 8 but also show two orthogonally-polarized fields between port1 and port2 of the proposed design.

The corresponding, far-field, 3-D radiation patterns of the loop studied in Fig. 9(a) are presented in Fig. 9(b). For port1 excitation, the radiation pattern resembles that of a dipole antenna placed along the axial direction ($\pm z$ axes), whereas the pattern for port2 excitation is similar to that of a horizontally

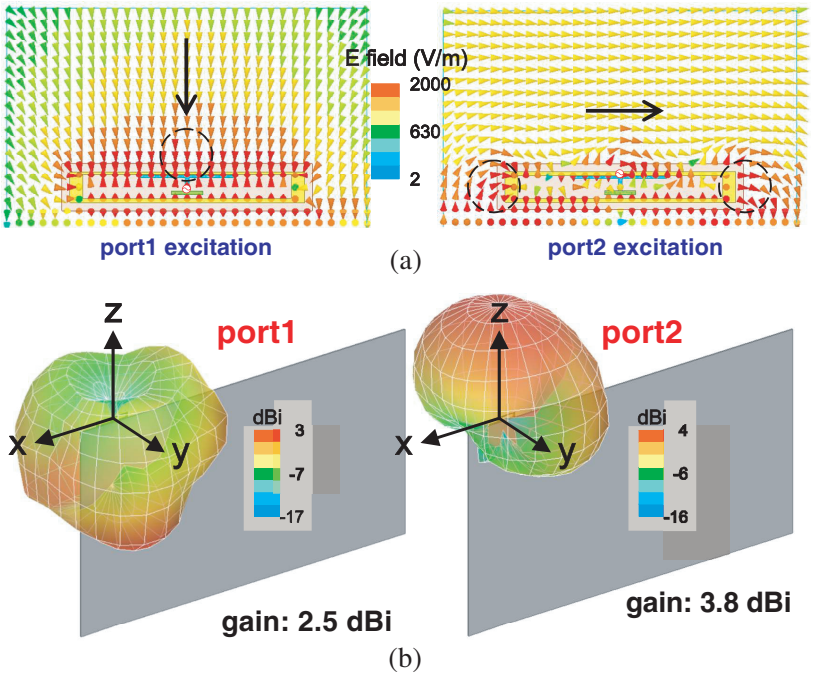

Figure 9. (a) Simulated electric field distribution and (b) 3-D radiation patterns of port1 and port2 of the proposed design excited at 3.5 GHz.

placed dipole along the $\pm x$ axes above a relatively large ground plane. Two radiation patterns showing orthogonal polarization with pattern diversity [30] are also very clear to see. Note that the peak gain of the proposed loop with port2 excitation is larger than that with port1 excitation by 1.3 dBi. This is because the one-wavelength loop, when port2 is excited, also functions as a folded dipole antenna [31] with maximum gain perpendicular to the antenna. In this case, the large display plate acts more like a reflector, aiming more antenna radiation in the $+z$ direction.

Figures 10(a) and (b) plot the measured and simulated 2-D radiation patterns in E-total field at 3.5 GHz for port1 and port2, respectively. Other frequencies were also measured in the 3.4–3.6 GHz band. Stable patterns were observed. Instead of separate polarization in E_θ and E_φ fields, it has

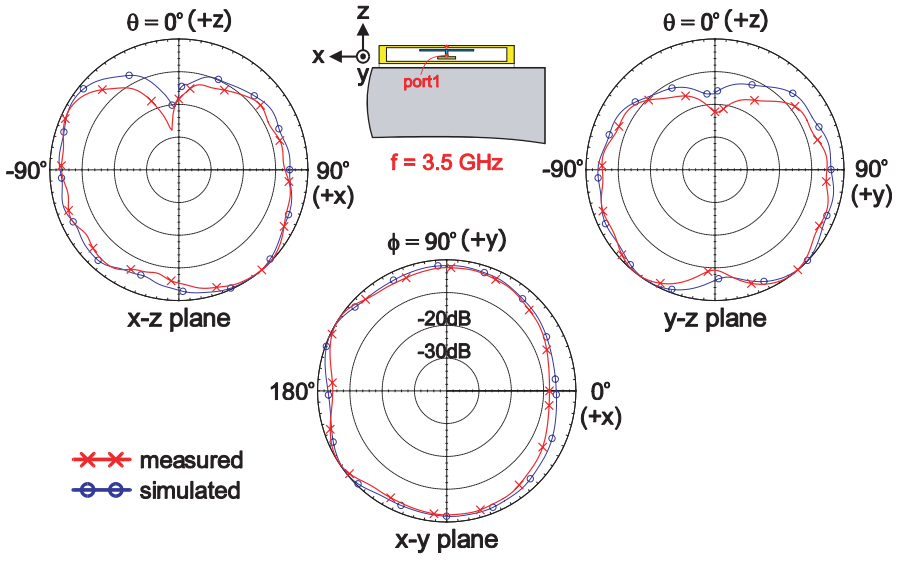

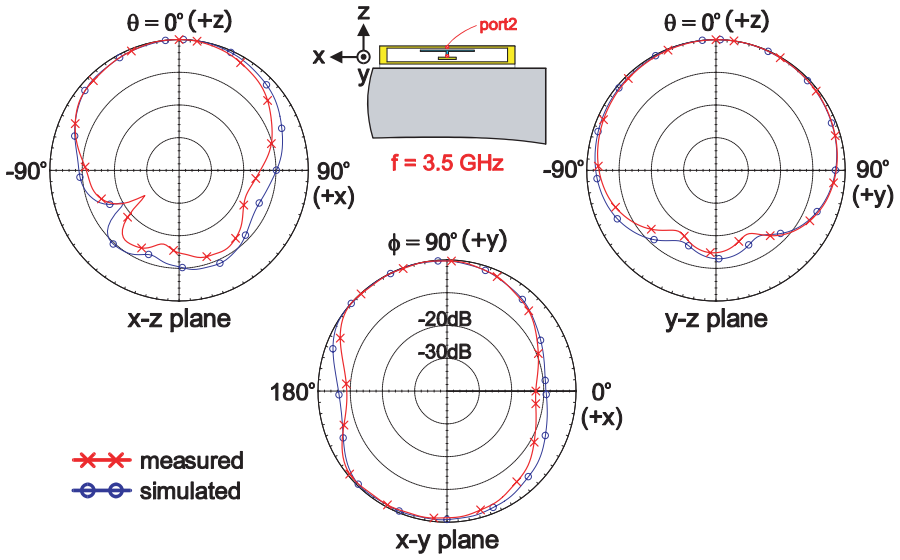

(b)

Figure 10. Measured and simulated 2-D radiation patterns (E-total) of (a) port1 and (b) port2 in the proposed design at 3.5 GHz.

been shown from our empirical studies on laptop wireless test results that the E-total patterns can determine the data throughput performance. It is because both vertical and horizontal polarizations exist in the real indoor or urban environment. The patterns in Fig. 10 are normalized with respect to the maximum gain in each principal cut. The radiation performance was measured at our multi-probe systems, SATIMO SG 24 [32], which can measure the spectrum from 400 MHz up to 10 GHz. For port1 measurement, the counterpart port2 was terminated to a 50 Ω load, and vice versa. For port1 excitation, the omnidirectional patterns are obtained in the x-y plane with radiation null above the display plate in the $+z$ direction. By contrast, for port2 excitation, large radiation intensity is observed in the $+z$ direction with less pattern gain along the $\pm x$ axes than in the $\pm y$ directions. Moreover, both the y-z patterns of port1 and port2 excitation are seen symmetrical.

Figure 11 plots the measured and simulated antenna efficiencies. The measured antenna efficiency fairly agrees with the simulated results. The measured efficiency is about 50%–60% and 60%–70%, respectively, for port1 and port2 working in the 3.4–3.6 GHz band. The measurement took account of the cable loss and antenna mismatch. Note that the relatively small antenna efficiency of port1 excitation is owing to the opposite current distribution on the loop's longer edges (see Fig. 8), which cancels out near-field radiation and leads to reduced antenna efficiency and gain in the far field.

The calculated ECC between two ports of the proposed loop is shown in Fig. 12. The ECC calculates the Hermitian product of the two complex far fields [33] in a uniform multipath environment of balanced polarization (that's, a Rayleigh fading channel) [29]. It reflects the similarity between the antenna radiation performance and the diversity of the two antennas. The calculation is defined as

$$\rho_e = \frac{\left| \iint_{4\pi} \left[\vec{E}_1(\theta,\phi) \cdot \vec{E}_2(\theta,\phi) d\Omega \right] \right|^2}{\iint_{4\pi} \left| \vec{E}_1(\theta,\phi) \right|^2 d\Omega \iint_{4\pi} \left| \vec{E}_2(\theta,\phi) \right|^2 d\Omega} \tag{2}$$

where the product of the two electric fields on the numerator can be given by

$$\vec{E}_1(\theta,\phi) \cdot \vec{E}_2(\theta,\phi) = E_{\theta 1}(\theta,\phi) E^*_{\theta 2}(\theta,\phi) + E_{\phi 1}(\theta,\phi) E^*_{\phi 2}(\theta,\phi) \tag{3}$$

in which the asterisk ($*$) sign of the E_θ and E_φ fields radiated by antenna 2 denotes the complex conjugate of the imaginary parts. The ECC is very low and less than 0.002 in the 3.4–3.6 GHz band. For mobile devices, the ECC less than 0.5 [34, 35] is considered low for good antenna diversity gain. It

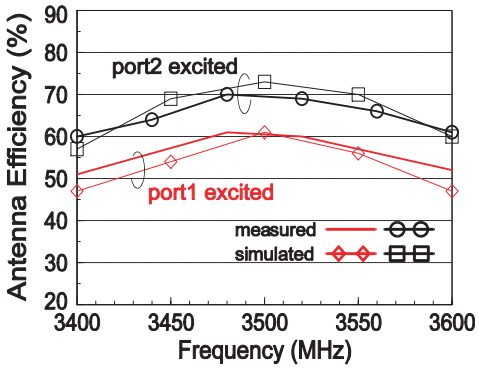

Figure 11. Measured and simulated antenna efficiency of port1 and port2.

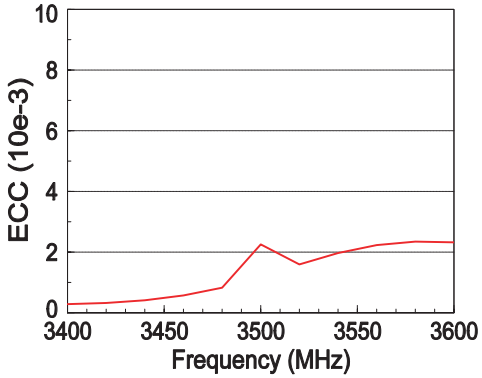

Figure 12. Calculated ECC between port1 and port2 excitation.

is also known that a lower envelope correlation suggests a larger channel capacity. The diversity gain based on the following calculation [36] is expected to be about 10 dB.

$$DG = 10\sqrt{1 - (ECC)^2} \tag{4}$$

4. CONCLUSION

A printed, two-port loop antenna having a compact size of 30 mm × 4 mm and very low transmission coefficient (S_{12}) between two ports lower than −32 dB for producing two uncorrelated waves of orthogonal polarization and pattern diversity has been proposed. A design example functioning in the 3.4–3.6 GHz band for 5G laptop applications has been demonstrated. The two ports, namely port1 and port2, of the loop are fed by a coupling strip and a direct feed, respectively, to excite the loop's two one-wavelength resonant modes. Based on this feeding mechanism, two orthogonal, folded-dipole-like waves can be attained, covering complementary radiation space with very low ECC of less than 0.002 in the frequency band of interest. Despite port2 having larger antenna efficiency/gain than port1, the diversity gain is expected to reach 10 dB. The proposed dual-polarized loop is of great interest to narrow-bezel laptop antennas in the 5G communications.

REFERENCES

1. Kurup, D. G., A. Rydberg, and M. Himdi, "Compact microstrip-T coupled patch antenna for dual polarisation and active antenna applications," *Electronics Lett.*, Vol. 38, 1240–1241, 2002.
2. Wong, K. L. and T. W. Chiou, "Finite ground plane effects on broadband dual polarized patch antenna properties," *IEEE Trans. Antennas Propagat.*, Vol. 51, 903–904, 2003.
3. Wong, H., K. L. Lau, and K. M. Luk, "Design of dual-polarized L-probe patch antenna arrays with high isolation," *IEEE Trans. Antennas Propagat.*, Vol. 67, 45–52, 2004.
4. Gao, S. and A. Sambell, "Dual-polarized broad-band microstrip antennas fed by proximity coupling," *IEEE Trans. Antennas Propagat.*, Vol. 53, 526–530, 2005.
5. Ryu, K. S. and A. A. Kishk, "Wideband dual-polarized microstrip patch excited by hook shaped probes," *IEEE Trans. Antennas Propagat.*, Vol. 56, 3645–3649, 2008.
6. Yang, S. L., K. M. Luk, H. W. Lai, A. A. Kishk, and K. F. Lee, "A dual-polarized antenna with pattern diversity," *IEEE Trans. Antennas Propagat. Mag.*, Vol. 50, 71–79, 2008.
7. Wei, K., Z. Zhang, W. Chen, and Z. Feng, "A novel hybrid-fed patch antenna with pattern diversity," *IEEE Antennas Wireless Propagat. Lett.*, Vol. 9, 562–565, 2010.
8. Sun, L., G. X. Zhang, B. H. Sun, W. D. Tang, and J. P. Yuan, "A single patch antenna with broadside and conical radiation patterns for 3G/4G pattern diversity," *IEEE Antennas Wireless Propagat. Lett.*, Vol. 15, 433–436, 2015.

9. Wang, Y. and D. Piao, "A dual-polarized antenna with pattern diversity based on a two-mode single-layer microstrip patch," *Proc. IEEE MTT-S Int. Wireless Symposium*, 1–3, Chengdu, China, 2018.
10. WRC-Press Release, World Radiocommunication Conference Allocates Spectrum for Future Innovation, http://www.itu.int/net/pressoffice/press_releases /2015/56.aspx.
11. Su, S. W., Y. T. Hsieh, and S. C. Chen, "Integration of very-low-profile slot antenna into notebook metal cover with narrow bezel," *Proc. Int. Symposium on Antennas and Propagat.*, 1–2, Phuket, Thailand, 2017
12. Su, S. W., "Very-low-profile, 2.4/5-GHz WLAN monopole antenna for large screen-to-body-ratio notebook computers," *Microw. Opt. Technol. Lett.*, Vol. 60, 1313–1318, 2018.
13. Su, S. W., C. T. Lee, and S. C. Chen, "Compact, printed, tri-band loop antenna with capacitively-driven feed and end-loaded inductor for notebook computers," *IEEE Access*, Vol. 6, 6692–6699, 2018.
14. Su, S. W., C. T. Lee, and S. C. Chen, "Very-low-profile, triband, two-antenna system for WLAN notebook computers," *IEEE Antennas Wireless Propagat. Lett.*, Vol. 17, 1626–1629, 2018.
15. Su, S. W., C. T. Lee, and Y. W. Hsiao, "Compact two-inverted-F-antenna system with highly integrated π-shaped decoupling structure," *IEEE Trans. Antennas Propagat.*, Vol. 67, 6182–6186, 2019.
16. Ansys HFSS, ANSYS Inc., https://www.ansys.com/products/electronics/ ansys-hfss.
17. Wong, K. L. and M. T. Chen, "Small-size LTE/WWAN printed loop antenna with an inductively coupled branch strip for bandwidth enhancement in the table computer," *IEEE Trans. Antennas Propagat.*, Vol. 61, 6144–6151, 2013.
18. Wong, K. L., C. Y. Tsai, and J. Y. Lu, "Two asymmetrically mirrored gap-coupled loop antennas as a compact building block for eight-antenna MIMO array in the future smartphone," *IEEE Trans. Antennas Propagat.*, Vol. 65, 1765–1778, 2017.
19. Li, Y., C.-Y.-D. Sim, Y. Luo, and G. Yang, "12-port 5G massive MIMO antenna array in sub-6GHz mobile handset for LTE bands 42/43/46 applications," *IEEE Access*, Vol. 6, 344–354, 2017.
20. Chang, W. H., S. W. Su, and B. C. Tseng, "Self-decoupled, 5G NR77/78/79 two-antenna system for notebook computers," *Electrical Design of Advanced Packaging and Systems*, 1–3, Kaohsiung, Taiwan, 2019.
21. Sun, L., Y. Li, Z. Zhang, and H. Wang, "Self-decoupled MIMO antenna pair with shared radiator for 5G smartphones," *IEEE Trans. Antennas Propagat.*, Vol. 68, 3423–3432, 2020.
22. Chen, S. C., L. C. Chou, C. G. Hsu, and S. M. Li, "Compact sub-6-GHz four-element MIMO slot antenna system for 5G tablet devices," *IEEE Access*, Vol. 8, 154652–154662, 2020.
23. Sun, L., Y. Li, and Z. Zhang, "Wideband integrated quad-element MIMO antennas based on complementary antenna pairs for 5G smartphones," *IEEE Trans. Antennas Propagat.*, Vol. 69, 4466–4474, 2021.
24. Su, S. W., "Printed loop antenna integrated into a compact, outdoor WLAN access point with dual-polarized radiation," *Progress In Electromagnetics Research C*, Vol. 19, 25–35, 2011.
25. Wan, C. C. and S. W. Su, "Compact, self-isolated 2.4/5-GHz WLAN antenna for notebook computer applications," *Progress In Electromagnetics Research M*, Vol. 83, 1–8, 2019.
26. Browne, D. W., M. Manteghi, M. P. Fitz, and Y. Rahmat-Samii, "Experiments with compact antenna arrays for MIMO radio communications," *IEEE Trans. Antennas Propagat.*, Vol. 54, No. 11, 3239–3250, 2006.
27. Chae, S. H., S. K. Oh, and S. O. Park, "Analysis of mutual coupling, correlations, and TARC in WiBro MIMO array antenna," *IEEE Antennas Wireless Propagat. Lett.*, Vol. 6, 122–125, 2007.
28. Su, S. W., C. T. Lee, and F. S. Chang, "Printed MIMO-antenna system using neutralization-line technique for wireless USB-dongle applications," *IEEE Trans. Antennas Propagat.*, Vol. 60, 456–463, 2012.
29. Sharawi, M. S., "Printed multi-band MIMO antenna systems and their performance metrics," *IEEE Antennas and Propagat. Mag.*, Vol. 55, 218–232, 2013.

30. Dietrich, C. B., K. Dietze, J. R. Nealy, and W. L. Stutzman, "Spatial, polarization, and pattern diversity for wireless handheld terminals," *IEEE Trans. Antennas Propagat.*, Vol. 49, 1271–1281, 2001.
31. Buxton, C. G., W. L. Stutzman, R. R. Nealy, and A. M. Orndorff, "The folded dipole: A self-balancing antenna," *Microw. Opt. Technol. Lett.*, Vol. 29, 155–160, 2001.
32. SATIMO SG 24, MVG, http://www.mvg-world.com/en/products/antenna- measurement/multi-probe-systems/sg-24.
33. Blanch, S., J. Romeu, and I. Corbella, "Exact representation of antenna system diversity performance from input parameter description," *Electronics Lett.*, Vol. 39, 705–707, 2003.
34. Vaughan, R. G. and J. B. Andersen, "Antenna diversity in mobile communications," *IEEE Trans Vehicular Technol.*, Vol. 36, 149–172, 1987.
35. Jha, K. R. and S. K. Sharma, "Combination of MIMO Antennas for handheld devices," *IEEE Antennas and Propagat. Mag.*, Vol. 60, 118–131, 2018.
36. Sharawi, M. S., *Printed MIMO Antenna Engineering*, Artech House, 2014.